JOURNAL OF THE ROYAL SOCIETY Interface

rsif.royalsocietypublishing.org

Research

Cite this article: Lim YF, Williams MAK, Lentle RG, Janssen PWM, Mansel BW, Keen SAJ, Chambers P. 2013 An exploration of the microrheological environment around the distal ileal villi and proximal colonic mucosa of the possum (*Trichosurus vulpecula*). J R Soc Interface 10: 20121008.
http://dx.doi.org/10.1098/rsif.2012.1008

Received: 6 December 2012
Accepted: 17 January 2013

Subject Areas:
biomechanics

Keywords:
microrheology, mucosa, ileum, colon

Author for correspondence:
R. G. Lentle
e-mail: r.g.lentle@massey.ac.nz

Electronic supplementary material is available at http://dx.doi.org/10.1098/rsif.2012.1008 or via http://rsif.royalsocietypublishing.org.

Royal Society Publishing
Informing the science of the future

An exploration of the microrheological environment around the distal ileal villi and proximal colonic mucosa of the possum (*Trichosurus vulpecula*)

Y. F. Lim[1], M. A. K. Williams[2,3,5], R. G. Lentle[1,3], P. W. M. Janssen[1], B. W. Mansel[2,5], S. A. J. Keen[2,5] and P. Chambers[4]

[1]Institute of Food, Nutrition and Human Health, [2]Institute of Fundamental Sciences, [3]Riddet Institute, and [4]Institute of Veterinary, Animal and Biomedical Sciences, Massey University, Private Bag 11222, Palmerston North, New Zealand
[5]MacDiarmid Institute of Advanced Materials and Nanotechnology, Wellington, New Zealand

Multiple particle-tracking techniques were used to quantify the thermally driven motion of ensembles of naked polystyrene (0.5 μm diameter) microbeads in order to determine the microrheological characteristics around the gut mucosa. The microbeads were introduced into living *ex vivo* preparations of the wall of the terminal ileum and proximal colon of the brushtail possum (*Trichosurus vulpecula*). The fluid environment surrounding both the ileal villi and colonic mucosa was heterogeneous; probably comprising discrete viscoelastic regions suspended in a continuous Newtonian fluid of viscosity close to water. Neither the viscosity of the continuous phase, the elastic modulus (G') nor the sizes of viscoelastic regions varied significantly between areas within 20 μm and areas more than 20 μm from the villous mucosa nor from the tip to the sides of the villous mucosa. The viscosity of the continuous phase at distances further than 20 μm from the colonic mucosa was greater than that at the same distance from the ileal villous mucosa. Furthermore, the estimated sizes of viscoelastic regions were significantly greater in the colon than in the ileum. These findings validate the sensitivity of the method and call into question previous hypotheses that a contiguous layer of mucus envelops all intestinal mucosa and restricts diffusive mass transfer. Our findings suggest that, in the terminal ileum and colon at least, mixing and mass transfer are governed by more complex dynamics than were previously assumed, perhaps with gel filtration by viscoelastic regions that are suspended in a Newtonian fluid.

1. Introduction

The fluid environment near the wall of the small intestine has a significant effect on the absorption of nutrients [1–3]. A body of experimental work shows that the rates at which soluble substances are passively absorbed from the lumen [4–6] are generally slower than those that would be expected from simple direct diffusion through the surface of the enteral mucosa. It has been suggested that this could result from the effect of a so-called unstirred water layer (UWL) interposed between the lumen and the surface of the enterocytes, which restricts diffusion [7–9]. The operational thickness of such an UWL has been estimated from transport measurements to be 74–600 μm in the small intestine, depending on the measurement technique, the rate at which the intestinal lumen is perfused [1,2,10–13] and the molecular volume of the solute [14].

While it is conceivable that such a UWL results largely from a continuous layer of mucus enveloping the intestinal epithelium [15,16], a number of findings run contrary to this hypothesis. Firstly, a number of workers have

reported that there are significant discontinuities in the mucus layer within several sites of the small intestine [17]. Secondly, direct measurements of the thickness of the layer of mucus overlying the apices of enterocytes do not consistently reflect the calculated thickness of the UWL obtained from the rates of transport of nutrients [18,19].

The work reported here uses multiple particle-tracking techniques to determine the patterns of local variation in the rheological properties at multiple sites in close proximity to living small and large intestinal mucosa, while avoiding the physical disruption of the mucin layer [20]. One aim was to determine whether the patterns fit in with the hypothesis of a contiguous layer of viscoelastic material partitioning the lumen contents from the mucosa. The disposition and rheological properties at sites adjacent to the apical and lateral surfaces of the villi in the terminal ileum of the brushtail possum (*Trichosurus vulpecula*) were compared with those at sites adjacent to the colonic mucosa, which is of markedly different morphology [18,21].

2. Material and methods

It is known that villous intestinal mucosa can be maintained *ex vivo* for significant periods of time, provided it is well oxygenated and adequately supplied with nutrients [22]. We used mucosa from the digestive tract of the brushtail possum as in this species both the small intestine and proximal colon are of simple tubular configuration and of a diameter suitable for attachment to our superfusion apparatus. Further, the tissues are robust, can readily be maintained in an organ bath, and the tubular form and length of the ileal villi (560 ± 10 μm; our observations) are similar to those in the human small intestine (500–1000 μm) [23,24]. All studies were conducted on tissue maintained *ex vivo* in carboxygenated Earles-Hepes buffer solution (HBS) as we had found in prior work that the mucosa promptly secreted copious quantities of mucus whenever it became anoxic.

2.1. Preparation of intestinal samples

Nine freshly trapped brushtail possums, of either sex and between 2 and 3 kg body weight, were each fasted for a minimum of 4 h and subsequently anaesthetized in an induction chamber with 5 per cent halothane in 33 per cent oxygen and 66 per cent nitrous oxide. Following induction they were maintained on a mixture of 1.5 per cent halothane in oxygen and nitrous oxide administered via a face mask attached to a Bain's circuit. The gut was accessed via a ventral midline abdominal incision. In six possums, a 20 cm length of the terminal ileum up to and including the ileocaecal junction was excised. In a further three possums, a 15 cm length of proximal colon immediately distal to the ileocaecal junction was excised. The possums were subsequently euthanized with intracardiac pentobarbitone (125 mg kg^{-1}).

The segment of excised gut was opened by a lengthwise cut and immediately placed with mucosa uppermost in carboxygenated HBS solution (composition in mM: NaCl, 124; KCl, 5.4; $MgSO_4$, 0.8; NaH_2PO_4, 1.0; $NaHCO_3$, 14.3; Hepes, 10; $CaCl_2$, 1.8 and glucose, 5.0) maintained at 37°C. This procedure diluted any adherent digesta and allowed it to float clear of the mucosal surface. A 2 cm^2 piece of mucosa and adherent wall was cut from this with its centre at 10 cm from the distal end of the section of terminal ileum or at 10 cm from the proximal end of the section of proximal colon, and tied over the 5 mm diameter sintered tip of the central tube in the superfusion apparatus (figure 1) with the mucosal surface outermost. This whole procedure was undertaken with due care to avoid any direct mechanical stimulation of the mucosa. A 100 μl aliquot of a suspension of fluorescent microbeads (0.5 μm) was applied to the mucosa and left *in situ* for 1 min to allow the microbeads to settle onto the mucosal surface. The tube was then installed in the superfusion apparatus (figure 1) with its tip immersed in a cylindrical bath so that the exposed mucosal surface and associated fluid were in the focal plane of an inverted fluorescence microscope (Nikon Eclipse TE2000-U). A 0.5 ml dose of verapamil solution was then added to the bath to inhibit any spontaneous smooth muscle induced movement in the tissue, which could interfere with the observation of Brownian motion.

The bath was perfused at 500 ml min^{-1} with carboxygenated (95% O_2 to 5% CO_2) HBS (figure 1) maintained at a temperature of 37°C. The bath had a capacity of 70 ml and excess HBS overflowed the rim into an outer compartment from where it was recirculated. HBS was also drawn at 2 ml min^{-1} through the sintered tip of the tube adjacent to the point where the excised gut wall was tied. The apparatus was designed so that shear rates would not approach those encountered *in vivo* [25] and any flow-induced mucin loss would be likely to be lower than that encountered *in vivo*.

The microscope was mounted on an air-damped table and equipped with a mercury fluorescent lamp (X-cite Series 120PC EXFO) and a 20×0.75 NA objective lens (CFI Plan Apo VC 20x). Image sequences were recorded with a Foculus FO124SC CCD camera. Bath circulation was halted 20 s before the commencement of imaging to prevent any flow-induced oscillation of the beads. The assumption that all bulk motion in the organ bath had ceased after 20 s was validated by the finding that the diffusivity of the microbeads was not detectably correlated with time. Image sequences were recorded for approximately 10 s at a frame rate of 20–43 Hz depending on the clarity of the microbeads and villi or epithelium surface. It was not possible to conduct observations for periods longer than 10 s as microbeads in regions of low viscosity tended to move out of the focal plane after longer periods of time. Circulation of HBS was reestablished on completion of several image sequences and maintained for a minimum of 5 min before further sequences were recorded.

At the conclusion of each experiment, the mucosa was removed from the tip of the probe and preserved in 10 per cent formal saline pending histological processing, sectioning and staining with haematoxylin and eosin. Representative stained sections were subsequently examined for signs of necrosis.

2.2. Microrheological technique

The passive microrheological analysis used in this study enables fragile local environments that are of restricted volume [26] to be explored without disruption and has been used previously to characterize mucus microenvironments in the cavities of the small intestine and airways [27–29].

In each frame, x–y coordinate data were extracted for the ensemble of microbeads using a Gaussian weighted polynomial fit to the image intensity [30]. It was not possible to survey Brownian motion directly in three dimensions as such a procedure would need to rely on consistent changes in the appearance of microbeads along the z-axis as a function of their distance from the focal plane of the microscope. Such consistency could be achieved with homogeneous fluids but not with suspensions of translucent material such as mucin as their translucence would confound the consistency of this variation. However, the two-dimensional analysis used in our work was subsequently validated by the results showing isotropy in the three dimensions insofar as there were no significant differences in the viscosities of the continuous phase between ensembles of microbeads measured around villi with their long axes orientated in the

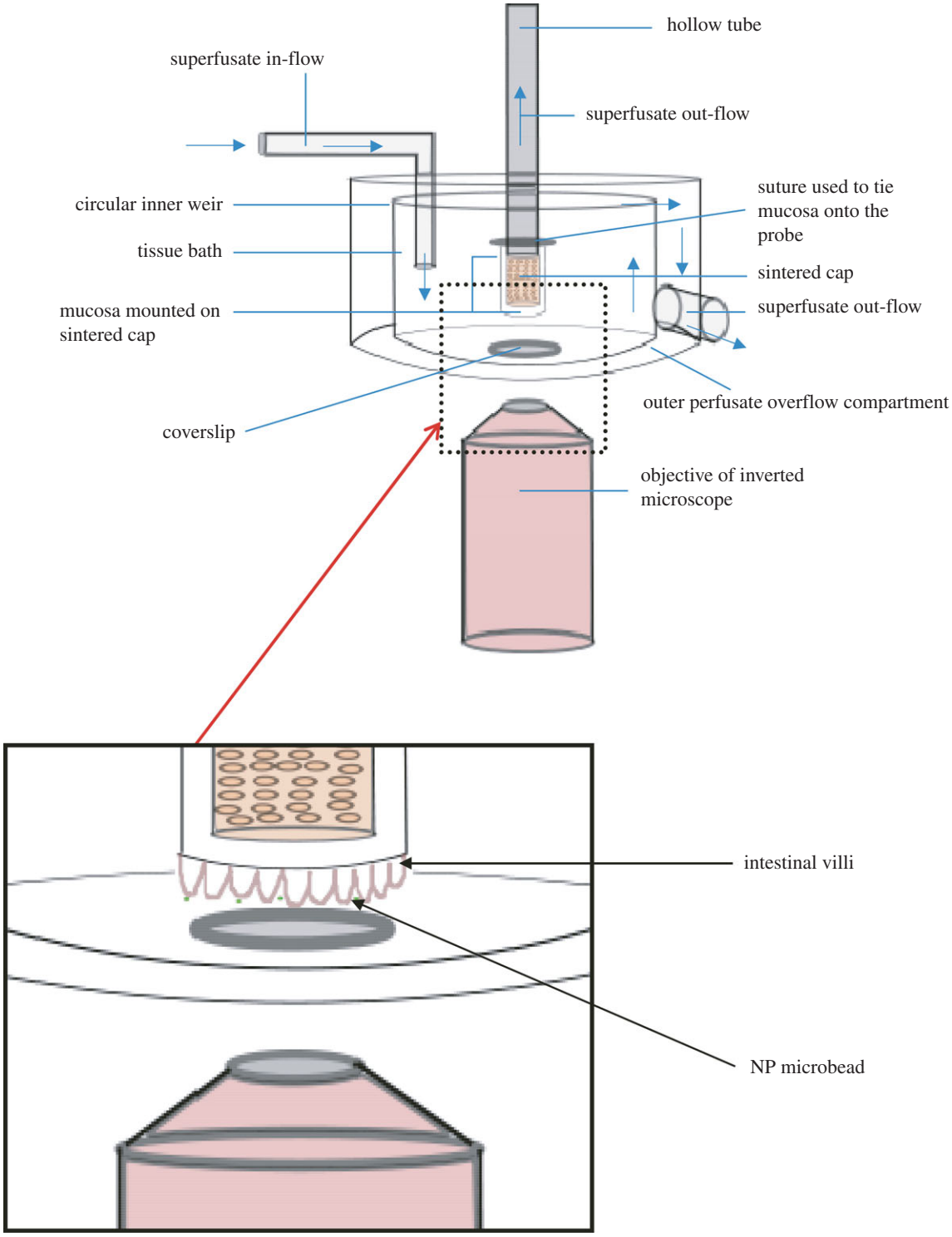

Figure 1. Organ bath. The excised mucosal tissue is mounted with villous surface outermost on the sintered tip of the hollow tube at the centre of the organ bath. The focal plane of the objective can be adjusted to lie at different points along the axes of the projecting villi. The circular weir allows carboxygenated HBS superfusate to overflow into the outer compartment with minimal turbulence.

x–z plane and those measured around villi with their long axes orientated in the x–y plane.

Any microbeads that exhibited excessive movement in the z-plane, i.e. moved with respect to the focal plane, were omitted. The data from a given microbead were only retained if it could be tracked over the course of 75–150 successive frames, depending on the frame rate. In addition, microbeads were tracked only if they were identified as single particles and did not exhibit intimate interactions with other beads. The temporal resolution of the tracking was limited by the frame rate of the camera (1/43 Hz) and the spatial resolution of the centre-of-mass movement of the tracer particles was estimated from control experiments to be around 5 nm for the tracking algorithm used.

The mean squared displacement (MSD or $\langle \gamma^2(\tau) \rangle$) of a microbead in the x–y plane was calculated from the x–y data using:

$$\langle \gamma^2(\tau) \rangle = \langle [x(t+\tau) - x(t)]^2 + [y(t+\tau) - y(t)]^2 \rangle, \qquad (2.1)$$

where τ is the lag time over which the mean squared displacement is determined, t is time, and x and y are the coordinates of the microbead [31]. The ensemble averaged MSD of microbeads undertaking thermally driven diffusive movement increases as a power

law with lag time:

$$\mathrm{MSD} \propto \tau^{\alpha}, \tag{2.2}$$

where α is the exponent [32]. In a purely viscous environment, the power-law exponent is 1 and hence, a plot of the logarithm of MSD against the logarithm of lag time yields a slope of 1. Conversely, should the diffusion of microbeads be hindered by interaction with an elastic structure surrounding it, then its diffusive movement will be restricted and the slope will be reduced [33].

For the purposes of this work, the microbeads were taken to be situated in a predominantly Newtonian fluid environment if the slopes of the log plots were in the range 0.8–1.1. In these situations, the viscosity could be meaningfully determined by extracting the diffusion coefficient using a linear plot and applying the Stokes–Einstein equation [32].

When the slopes of log plots were less than 0.8, the component microbeads were considered to be situated in a viscoelastic fluid environment. In these cases, the MSD data were transformed to obtain a viscoelastic spectrum using a modified generalized Stokes–Einstein (GSE) equation [26,32,33]. This spectrum contains information on the relative viscous and elastic components of the material as a function of a lag time. Elastic moduli (G') values were calculated at a frequency of 1 Hz as this value was within the physiological range likely to be encountered by digesta in the intestine [34,35].

2.3. Assessing the homogeneity of the environments of bead ensembles

The homogeneity of the fluid environment within which each bead ensemble was moving was assessed by examining the distribution of displacements of the microbeads in the x-direction after a given lag time. Frequency distributions of the different displacements found over the ensemble, also known as van Hove plots, were prepared [36]. For a homogeneous system, where all the beads experience the same mechanical environment, the different displacements sampled by the ensemble arise simply from the stochastic nature of Brownian motion and the data are expected to fit to a single Gaussian curve centred on the point of origin and with the variance equal to the MSD calculated at the relevant lag time. Similarly, data that clearly fits to a sum of two Gaussian curves, each centred on the origin but with different breadths, can be taken to indicate that the component microbeads were distributed in two different micromechanical environments (figure 2*a–c*). The suitability of such assignments was formally assessed by comparing the distribution pattern of residuals obtained after fitting with either a single or a double Gaussian function with Origin v. 8.5 software (OriginLab, Northampton, MA).

In cases where the method indicated that the beads in an ensemble were situated in a heterogeneous environment and were distributed between two regions of distinct mechanical properties, direct plots of microbead trajectories were prepared and these trajectories were colour-coded according to the magnitude of their displacements (figure 3*a*). Local homogeneity within each environment was then confirmed by plotting separate van Hove plots (figure 2*b*,*c*) of beads with MSDs of a given colour-coding and ensuring these were Gaussian.

These trajectory plots also enabled the location of the individual beads in each of the two environments to be distinguished (figure 3*a*) by the consistency of colour-coding. A box-counting algorithm (BCA) was then implemented in Matlab (Mathworks, Natick, MA) in order to examine areas of a particular colour-coding where the motions of microbeads were more highly restricted (figure 3*b*). The program evaluated the MSDs of all microbeads within a 'box' of set dimensions (128 × 96 pixels—one-fifth of the total visual field) that traversed the image in steps of five pixels by row and column, and determined the densities of particles that fell within the narrower Gaussian curve in the two-component van Hove plots as the box progressed across the image. The resulting map was colour-coded with dark red to yellow shadings indicating areas containing higher densities of microbeads with restricted, i.e. sub-diffusive, MSDs and with blue indicating areas with higher densities of beads exhibiting unrestricted, i.e. purely diffusive, MSDs. An area was termed a viscoelastic region only when an area shaded red to yellow contained three or more microbeads with restricted MSDs. The sizes of these viscoelastic regions were each estimated by determining the diameter of the largest circle centred on the geometric centre of the positions of the contributing microbeads that could be entirely contained within the 'viscoelastic' (red and yellow colour-coded) area. Only the diameters of regions whose boundaries did not come into contact with the edges of the visual field were determined.

The areas of viscoelastic regions as a percentage of the sampling area (0.064 mm^2) were also estimated by calculating the sums of the areas of the component circles within the sampling area based on these diameters.

2.4. Fluorescent microbeads

Naked polystyrene (NP) hydrophobic fluorescent microbeads (yellow fluorescent, excitation wavelength at 441 nm, emission at 486 nm) (Polysciences, Warrington, PA, USA) of 0.5 μm diameter were applied to preparations obtained from a total of six distal ilea and three proximal colons. These beads were chosen on the basis that their movements would be relatively restricted when they were located in mucins as they would adhere to hydrophobic regions of mucin proteins [37]. The size of beads was chosen to exceed the mean reported distance of around 100 nm between component strands of mucin [38] so as to prevent the sampling voids between adjacent strands of the mucin matrix [20]. Indeed, quantitative microrheology in such systems requires that the microbead size should be in excess of that of the polymer mesh.

2.5. Sampling and statistics

The viscosities of regions that exhibited Newtonian characteristics and the G' of regions that exhibited viscoelasticity were determined separately for sub-ensembles of microbeads, both at distances within 20 μm and at distances greater than 20 μm from the intestinal epithelium. This distance classification was chosen on the grounds that the adherent mucus layer is reported to extend 29 ± 8 μm from the surface of the ileum [18]. A similar distance classification was used for microbeads located in the colonic mucosal environment for the purposes of comparison.

A series of image sequences of microbead motion were obtained at multiple sites at different focal planes on a given sample of mucosa from a given animal over a period of 2 h. An image sequence at a particular site and focal plane was termed a replicate. Subsequent analysis was conducted on data from sites with a suitable density of microbeads and clarity of the villus edge.

The values obtained for the various parameters required transformation to render them suitable for parametric statistical analysis. This was carried out using the Johnson algorithm in the Minitab package (Minitab Inc., State College, PA, USA). Data were analysed by nested ANOVA for the effects of distance from mucosa, gut segment and animal) in the Systat package (Systat Software Inc., Chicago, IL, USA). Hence the results are presented as raw data in box plots in the text along with statistical inferences drawn from the ratio of mean squares from ANOVA of the overall effect to that of the effect nested within animal.

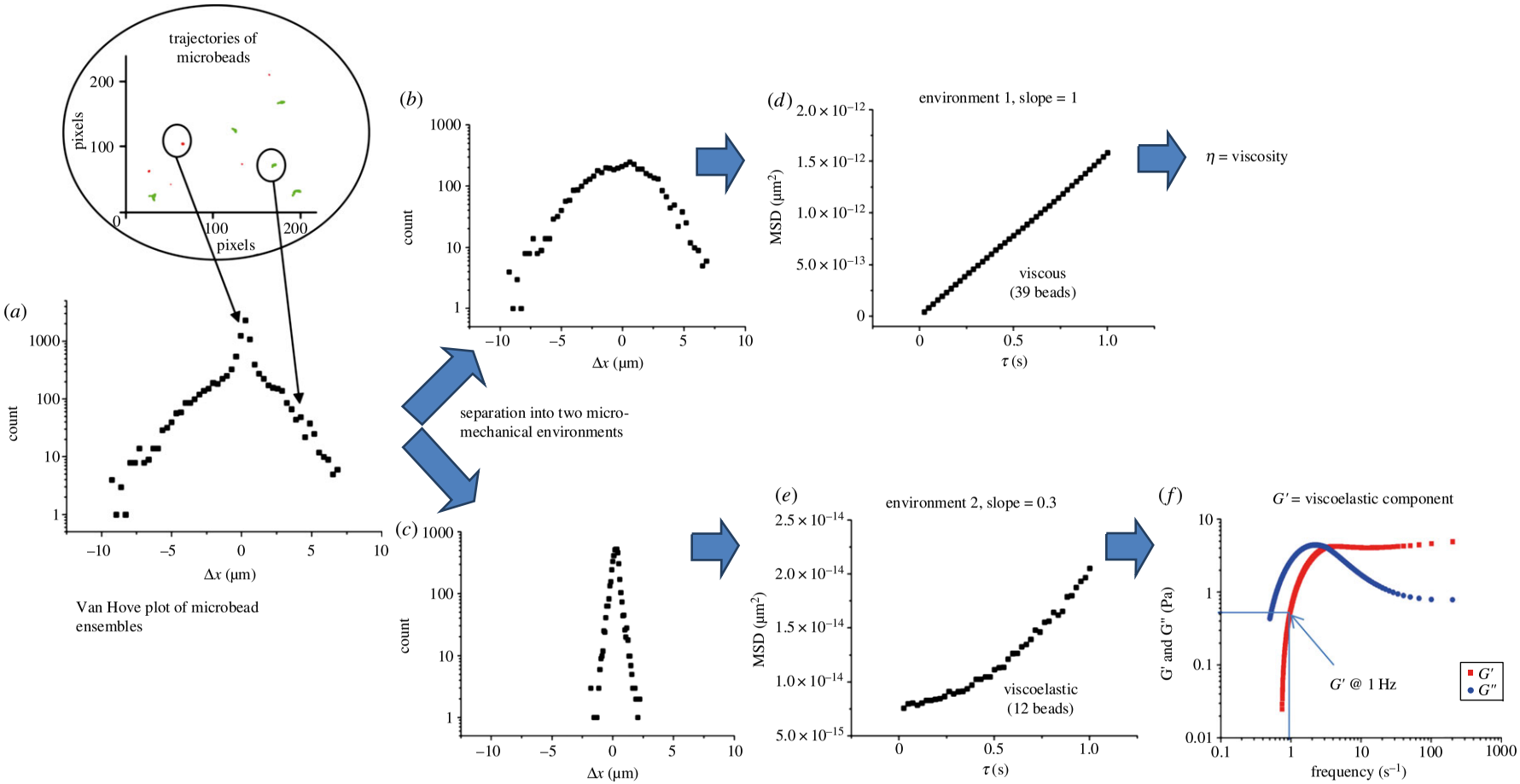

Figure 2. Spatial analyses of microrheological environments. An initial van Hove plot of the combined MSDs from the trajectories of all beads in a field showing a composite form (*a*). The data are better fitted by two Gaussian curves (*b,c*) than a single curve. Data from the broader curve (*b*) plotted as log MSD (micrometres) versus log lag time (*d*) yields a straight line indicating bead motion in a Newtonian fluid and allowing viscosity to be calculated from the slope. Data from beads in a viscoelastic region contribute to the narrower curve (*c*). Here a plot of log MSD (micrometres) versus log (*e*) yields a curve indicating viscoelasticity. In this case, G' (elastic modulus) and G'' (viscous modulus) can be derived (*f*).

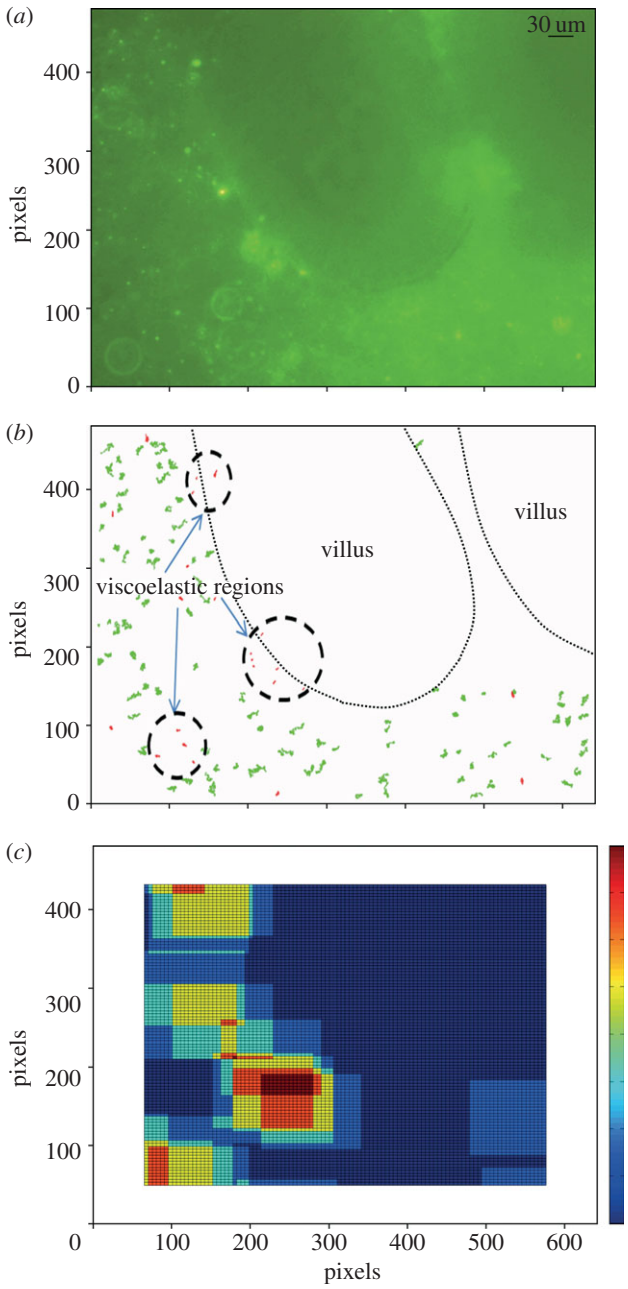

Figure 3. Mapping of viscoelastic regions. (*a*) Photomicrograph showing the location of the villi and the distribution of microbeads. (*b*) A direct plot of the trajectories of a field of microbeads allows the sub-diffusive trajectories (coded red) of beads within viscoelastic regions to be distinguished from the more extensive diffusive trajectories of microbeads (coded green) within the continuous fluid phase. (*c*) Output from the BCA that delineates viscoelastic regions containing groups of beads with sub-diffusive MSDs.

3. Results

The continuation of contractile activity in the walls of *ex vivo* preparation of the colon and terminal ileum for a period exceeding 1 h in a number of pilot experiments confirmed that the tissue remained viable for this time. Histological examination confirmed that the enterocyte epithelium had remained intact for the duration of the experiment and did not exhibit any signs of necrosis (figure 4). Moreover, numbers of mucin bearing goblet cells were evident within the mucosa indicating that there had been no general discharge of their contents stimulated by anoxia (figure 4).

Analyses of the behaviour of microbeads showed the environment around the ileal villi and the colonic mucosa were largely heterogeneous consisting of a continuous phase of Newtonian liquid that contained viscoelastic regions. The behaviour of ensembles of microbeads that exhibited average MSDs that scaled linearly with lag time and fitted with the broader of the two van Hove plots (figure 2*b*) indicated that they were situated in liquid and could be used to determine local viscosity (figure 2*d*). Similarly, the behaviour of ensembles of microbeads that exhibited average MSDs that varied with lag time according to a local power law (figure 2*e*) and fitted with the narrower of the two van Hove plots (figure 2*c*) indicated that they were situated in a viscoelastic material and could be used to determine elastic and viscous moduli. The dependence of the latter values upon frequency (or timescale) of perturbation was typical of that found in viscoelastic solutions of highly entangled polymer solutions [39].

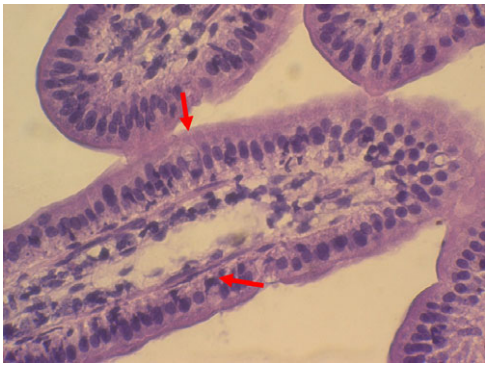

Figure 4. Stained section of villi from mucosal sample following passive microrheology. Stained sections show preservation of tissue structure with no evidence of necrosis (haematoxylin and eosin stain). The red arrows indicate mucin granules lying within intact goblet cells.

3.1. Ileal mucosa

The continuous phase of the environment around the terminal ileal villi was a Newtonian fluid of viscosity close to that of water (the viscosity of water measured by our methods was found to be close to 1 mPa's as expected). The overall median viscosity of the continuous phase obtained using pooled data from all ileal preparations (table 1 and figure 5*a*) was not significantly different on nested ANOVA at sites less than 20 µm to those at greater than 20 µm from the mucosa. The median viscosity of the continuous phase at sites that were greater than 20 µm above the apical epithelium of the villus tip (median value 1.49 mPa's; interquartile range (IQR) 1.08–2.06, $n = 15$ replicates) did not differ significantly from that at sites greater than 20 µm from the sides of the villus (median 1.34 mPa's; IQR 1.13–1.8, $n = 59$ replicates).

The median elastic modulus (G') of viscoelastic regions found in the continuous phase, obtained with pooled MSD data from all preparations, did not differ significantly between sites 20 µm or closer to the mucosa to that at sites further than 20 µm from the mucosa (table 1 and figure 5*b*). The diameters of viscoelastic regions further than 20 µm from the ileal epithelium did not differ significantly from those of regions situated 20 µm or closer to villus epithelium (table 1 and figure 6*a*).

The numbers of viscoelastic regions around the villous ileal epithelium were generally low. Of 26 replicates from sites that contained entire viscoelastic regions, the visual

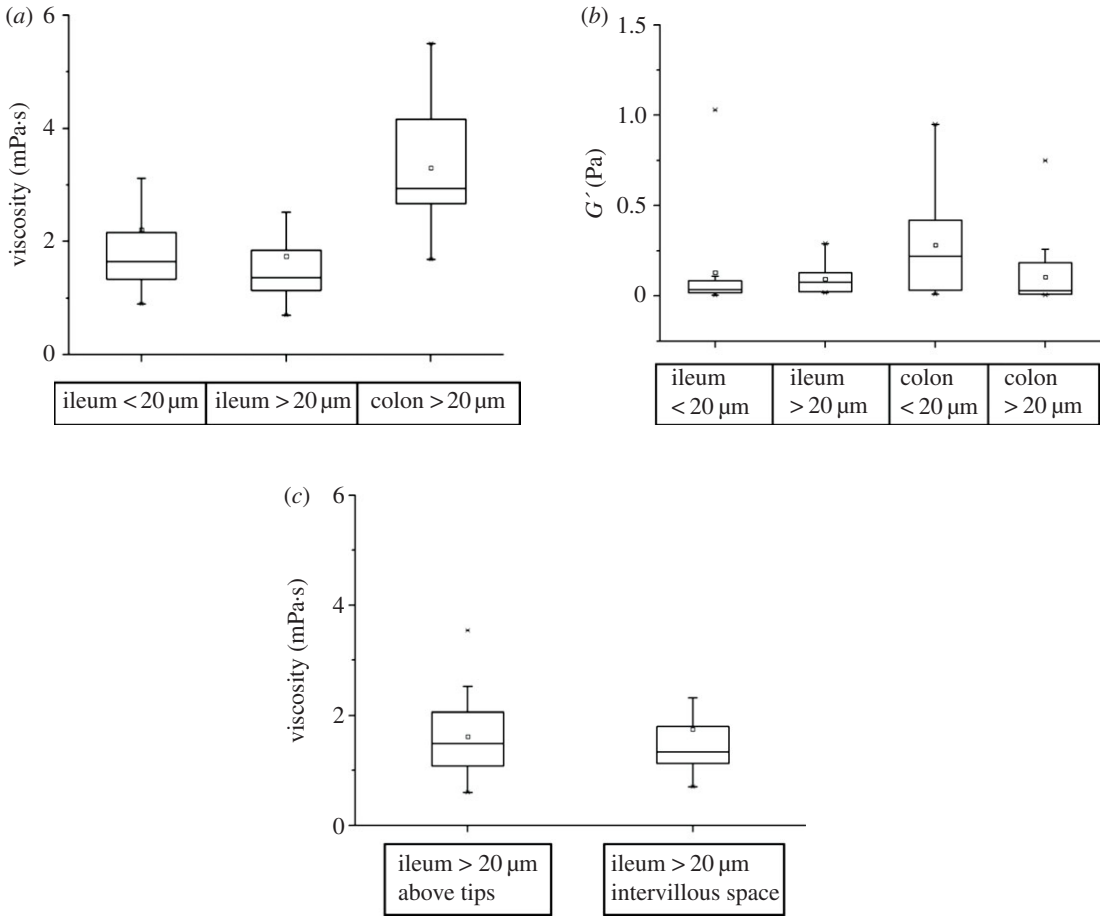

Figure 5. Variation in the rheological properties of the continuous phase and viscoelastic regions with intestinal segment, distance from the mucosa and location around intestinal villi (i.e. tips and sides of villi). (*a*) Viscosity of continuous phase, (*b*) elastic moduli of rafts (G'), (*c*) comparison of viscosity of continuous phase $>$ 20 µm from the tip and the sides of ileal villi.

Table 1. Summary of the microrheological properties (viscosity and elastic moduli) of the continuous phase of Newtonian fluid and viscoelastic regions, region diameters and percentage area occupied by viscoelastic regions per 0.064 mm^2 field of view.

measured parameter	site	*n* (replicates)	median	IQR
continuous Newtonian phase viscosity (mPa · s)	ileum < 20	50	1.68	1.34–2.18
	ileum > 20	66	1.35	1.14–1.85
	colon < 20	2		3.18–5.22[a]
	colon > 20	16	2.94	2.67–4.16
viscoelastic regions elastic moduli (Pa)	ileum < 20	19	0.036	0.017–0.085
	ileum > 20	10	0.077	0.023–0.13
	colon < 20	11	0.22	0.032–0.42
	colon > 20	20	0.03	0.01–0.19
viscoelastic regions diameter (µm)	ileum < 20	12	25.1	22.2–40
	ileum > 20	14	27.8	22.7–53
	colon < 20	12	48.4	34.1–52.9
	colon > 20	8	33.8	23.5–54
percentage of area occupied by viscoelastic regions per 0.064 mm^2 field of view	ileum < 20	12	0.78	0.6–2
	ileum > 20	14	0.85	0.6–1.1
	colon < 20	12	2.9	1.4–3.5
	colon > 20	8	1.4	0.7–3.7

[a]A range is given for this site as there were insufficient values for the calculation of median and IQR. It is included for comparison with other viscosity values.

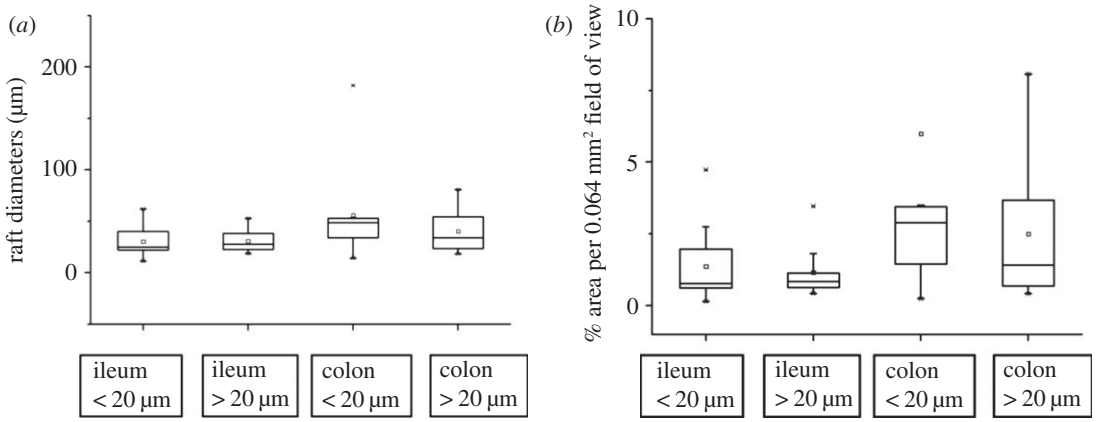

Figure 6. Variation in the diameter and projected area of viscoelastic regions near the ileal villous and colonic mucosa. (*a*) Variation between the ileum and colon in diameters of viscoelastic rafts, (*b*) variation between the ileum and colon in the areas of viscoelastic rafts.

fields in the majority contained one region per field of view while the visual field in one image sequence contained three regions and those in a further three sequences contained two regions. The percentage area per (0.064 mm^2) field of view occupied by viscoelastic regions in sites situated at a distance greater than 20 μm from the ileal mucosa did not differ significantly from that of those situated at 20 μm or closer to the surface of the ileal mucosa (table 1).

3.2. Colonic tissue

The viscosities of the continuous (Newtonian fluid) phase at sites that were situated further than 20 μm did not differ significantly from those 20 μm or closer to the colonic epithelium (table 1). No median and IQR value was available for the viscosity at sites 20 μm or less from the epithelium of the colon as the bulk of microbead ensembles (11 out of 13) were located in viscoelastic material and those in regions containing only Newtonian fluid were correspondingly low. However, these viscosity values were within the range of the values found in sites greater than 20 μm from the colonic epithelium.

The *G′* of viscoelastic regions situated in the continuous phase at sites greater than 20 μm from the colonic epithelium did not differ significantly from those of regions situated 20 μm or less from the colonic epithelium (table 1). The diameters of viscoelastic regions situated at sites greater than 20 μm from the colonic epithelium did not differ significantly to that of those situated 20 μm or less from the colonic epithelium (table 1).

The numbers of viscoelastic regions were generally low around the colonic epithelium. Of a total of 20 replicates from sites that contained entire regions, the bulk of fields contained a single region, six contained two regions and one contained three regions. The percentage areas of the fields of view (0.064 mm^2) that were occupied by regions at sites situated at a distance greater than 20 μm from the colonic mucosa did not differ significantly from that of those situated 20 μm or less from the colonic mucosa (table 1).

3.3. Comparison of ileum and colon

The viscosities of the continuous Newtonian phase obtained at locations that were 20 μm or more from the colonic mucosa were significantly greater than those obtained at locations that were 20 μm or more from the ileal villous epithelium on ANOVA (d.f. = 8,131, $F = 3.416$, $p < 0.01$; figure 5*a*). The viscosities of the continuous phase obtained at locations that were less than 20 μm from the ileal or colonic mucosa could not be compared because of insufficient data being obtainable from this site in the colon.

The values for *G′* obtained from viscoelastic regions that were situated 20 μm or closer to the colonic mucosa were not significantly different to the values obtained from regions situated 20 μm or closer to the ileal villous mucosa (figure 5*b*). Similarly, the values for *G′* obtained from regions that were situated at distances greater than 20 μm from the colonic mucosa were not significantly different to those obtained from regions situated at distances greater than 20 μm from the ileal villous mucosa (figure 5*b*).

The numbers of viscoelastic regions identified in each visual field were generally low regardless of their distance from the mucosa or the gut segment from which the image sequence was obtained (ileum or colon), the majority of sites contained only one region. However, while regions that were situated above the ileal mucosa were always surrounded by the continuous Newtonian fluid phase, a significant number of regions that were situated above the colonic mucosa filled the entire visual field and were also counted as a single viscoelastic region.

Taken overall, the diameters of the viscoelastic regions in the colon were significantly greater on ANOVA (d.f. = 5, 42, $F = 2.604$, $p = 0.05$) than those in the ileum. However, the lack of any significance in the term for distance within segment indicated that there was no significant variation in region size with distance from the surface of the mucosa in this analysis (figure 6).

3.4 Further corroborative work

A series of further experiments were conducted on distal ileal and colonic samples from nine possums that yielded a total of 99 image sequence replicates (63 of the ileal and 36 of the colonic mucosa) in which Brownian motion of amine-coated polystyrene beads of 0.75 μm in diameter could be evaluated in a similar manner to the foregoing work. These beads were chosen as they adhered to mucin by electrostatic rather than hydrophobic interaction. The results obtained from this further work did not differ significantly from those detailed above, showing similar disposition of viscoelastic regions of similar dimension in the two gut segments. A summary of

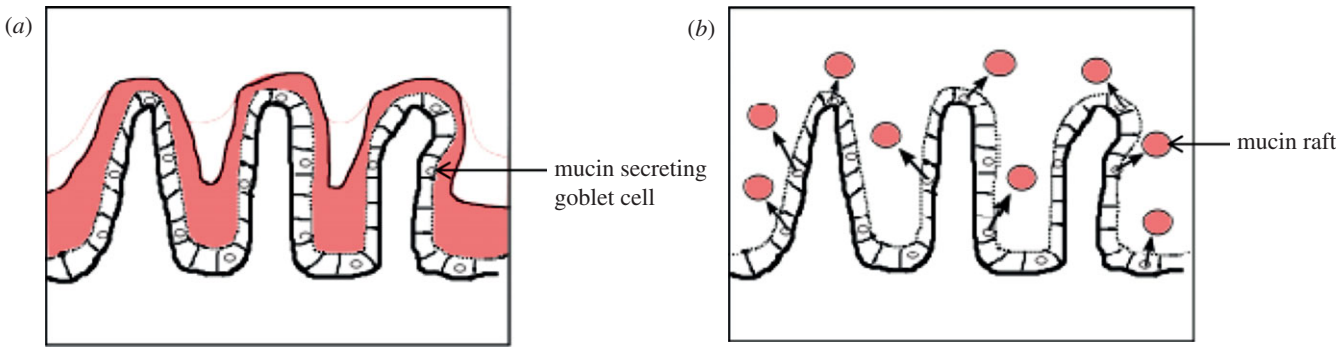

Figure 7. Alternate models for disposition of mucin around villi. (*a*) Extensive reptative interdiffusion between secreted mucin granules to form a continuous layer. (*b*) Limited reptative interdiffusion between secreted mucin of mucin granules leading to discontinuity.

the data from this work are available in the supplementary material (see the electronic supplementary material, figure S1).

4. Discussion

This is the first study to demonstrate that the material in sites immediately adjacent to the small and large intestinal mucosa is rheologically heterogeneous, comprising circumscribed regions that exhibit viscoelastic behaviour similar to that of purified mucus and contained within a more extensive phase of low viscosity Newtonian fluid. In principle, either one or both of the two phases could form a percolating network. As the low viscosity phase percolates across most of the two-dimensional images it is reasonable to conclude that this phase is contiguous in three-dimensional space. However, the viscoelastic phase does not percolate the two-dimensional images and occupies a low percentage of the area per field of view (0.78–0.85% in the ileum and 1.4–2.9% in the colon). Such low percentages would require generally thin linkages were this phase to percolate through three-dimensional space. The lack of any long and thin viscoelastic components suggests the viscoelastic regions are dispersed rather than linked.

In regard to the rheological characteristics of the continuous phase, it is important to note that observations of the motions of beads were restricted to periods of less than 10 s. Hence, it is possible that fluid in these regions could behave in a viscoelastic fashion over longer timescales, for example as a result of dispersal of extended molecules of mucin in dilute solution. However, given that flow within the intestinal lumen results from contractile events of short duration and is correspondingly short-lived, it is unlikely that such behaviour would be of physiological import.

While further work is required to relate the nature of viscoelastic regions to mucin secretions and their ability to anneal by reptative (snake-like diffusive motion of polymer chains within polymer entanglements [40]) inter-digitation of polymer chains on adjacent mucin masses, the results fit in with a number of previous reports that the intestinal mucus layer is discontinuous [17] (figure 7*b*). However, they run contrary to reports that the mucus layer forms a contiguous viscoelastic 'blanket' [41] (figure 7*a*) that overlies the absorptive surface of epithelial cells and restricts the rate at which nutrients are absorbed. The latter hypothesis is to some extent founded on the properties of mucins that have been 'purified' to remove cellular and other debris [15,27], and hence, may not reflect the heterogeneity that exists *in vivo*. Likewise, the lamellar structure of mucin found adjacent to the gastric [42] and colonic [43] mucosa may reflect a similar structure to that we report here, comprising stacks of discrete regions of mucin that have become compacted and distorted by histochemical and immunohistological processing. Previous evidence regarding the contiguity of the mucin 'blanket' is equivocal. The tendency of particles to agglomerate within the lumen after being applied to living intestinal mucosa [44] suggests the mucus layer is impenetrable, while work showing that a commensal species *Enterobacter cloacae*, which is not equipped to navigate viscoelastic mucin, is found in murine colonic crypts [44] suggests the discontiguity of this layer and supports our hypothesis.

Given that NP microbeads have been found to adhere strongly to mucus [28,29,41], our results suggest either that masses of mucin secreted by individual mucosal goblet cells do not always 'anneal' to neighbours [45] to form a contiguous layer, or that sites of translational diffusion and reptative inter-digitation of adjacent mucin masses are more vulnerable to digestion by enteral micro-flora. It is known that small variations in the structure of constituent mucin polymer chains can disrupt their configuration, obstructing reptative diffusion and impeding annealing [45]. Similarly, the presence of other high molecular weight polymers derived from nutrients can inhibit the expansion of mucin granules following their secretion by goblet cells [46,47].

Mucin granules from goblet cells in the respiratory epithelium of the rabbit are reported to expand 250-fold after their secretion [48]. The largest mucin granules within goblet cells are between 0.8 and 1.5 μm in size [49–51]. Hence, we may expect that the area of the expanded mucin from a single granule will lie between 100 and 370 μm^2. If viscoelastic regions found in our study consist principally of mucins this suggests that the aggregation of mucin granules is somewhat limited.

The heterogeneity of the microrheological environment around the colonic and villous small intestinal mucosa may explain the variation in the functional thickness of the 'UWL' with the molecular size of the probe [14]. Thus, larger molecules would tend to be more confined to the watery continuous phase while smaller molecules, which are able diffuse into viscoelastic regions, would be retained for longer in a process akin to gel filtration. The extent of this effect will depend on the width of the channels in the continuous phase. Our estimates of the percentage area per field of view of the viscoelastic regions suggest these channels are wide but this finding may have been influenced by a reduction in the rates at which water and contained nutrients

are absorbed in an *ex vivo* mucosal preparation where subsequent vascular transport is necessarily inhibited. These heterogeneous structures may similarly act to confine fat micelles to the continuous phase allowing them to penetrate more readily to the villous mucosa. Similarly, it may allow membrane vesicles exocytosed from the enterocyte brush border to bypass the mucin layer and enter the lumen [52].

The heterogeneous microrheological structure also has important consequences for the process of mixing within the intervillous space and our understanding of the transit and absorption of nanoparticles containing therapeutic substances that might adhere to viscoelastic regions [20,28,53]. While previous reports have indicated that mucins can accumulate in the intervillous space [18], the current work is the first to report the heterogeneous microrheology therein, its similarity to that around the villous tips suggesting that there is ongoing admixture and transit of these elements between the lumen and the intervillous spaces during longitudinal [54] and circular [55] contractile activity.

Our finding that viscoelastic regions are generally more extensive and the intervening continuous phase correspondingly reduced in sites less than 20 μm from the colonic epithelium, than at similar sites in the small intestine, suggest either that reptative diffusion and inter-digitation of polymer chains on adjacent mucin masses occurs more readily with colonic mucins, or that colonic viscoelastic regions are more mechanically resilient perhaps reflecting the greater diversity of colonic than small intestinal mucin structure [43,44,56]. The greater variance in the area and diameter of the regions is similarly likely to reflect differences in the capacity for reptative diffusion of the different colonic mucins. The finding that the continuous phase in the colon has a greater viscosity than that in the ileal environment may reflect a greater content of enteral micro-flora or concentration of oligosaccharides from bacterial degradation of dietary non-starch polysaccharides.

While the size and form of ileal villi of the possum are similar to those of humans and the mucosal architecture is broadly similar over the range of laboratory species, notably the density of villi and effective surface area per unit villus [57], it is possible that the spatial pattern of aggregation of secreted mucins varies between species. Hence, caution is required pending completion of similar studies at other sites and in other species. However, the results raise the possibility that the constituents of the mobile mucin layer are not always deployed to act as a contiguous barrier [58], that strategy perhaps being sacrificed in segments of the gut where absorption of residual nutrients is at a premium.

All procedures were approved by Massey University Animal Ethics Committee (approval no. 11/45).

References

1. Read NW, Levin RJ, Holdsworth CD. 1976 Proceedings: Measurement of the functional unstirred layer thickness in the human jejunum *in vivo*. *Gut* **17**, 387.
2. Westergaard H, Dietschy JM. 1974 Delineation of the dimensions and permeability characteristics of the two major diffusion barriers to passive mucosal uptake in the rabbit intestine. *J. Clin. Invest.* **54**, 718–732. (doi:10.1172/JCI107810)
3. Wilson FA, Sallee VL, Dietschy JM. 1971 Unstirred water layers in intestine: rate determinant of fatty acid absorption from micellar solutions. *Science* **174**, 1031–1033. (doi:10.1126/science.174.4013.1031)
4. Anderson BW, Levine AS, Levitt DG, Kneip JM, Levitt MD. 1988 Physiological measurement of luminal stirring in perfused rat jejunum. *Am. J. Physiol.* **254**, G843–G848.
5. Amidon GL, Kou J, Elliott RL, Lightfoot EN. 1980 Analysis of models for determining intestinal wall permeabilities. *J. Pharm. Sci.* **69**, 1369–1373. (doi:10.1002/jps.2600691204)
6. Levitt MD, Aufderheide T, Fetzer CA, Bond JH, Levitt DG. 1984 Use of carbon monoxide to measure luminal stirring in the rat gut. *J. Clin. Invest.* **74**, 2056–2064. (doi:10.1172/JCI111629)
7. Winne D. 1981 Unstirred layer as a diffusion barrier *in vitro* and *in vivo*. In *Intestinal absorption and secretion* (eds F Skadhause, K Heintse), pp. 21–38. Lancaster, UK: MTP Press.
8. Thomson AB, Dietschy JM. 1977 Derivation of the equations that describe the effects of unstirred water layers on the kinetic parameters of active transport processes in the intestine. *J. Theor. Biol.* **64**, 277–294. (doi:10.1016/0022-5193(77)90357-5)
9. Thomson ABR, Dietschy JM. 1984 The role of the unstirred water layer in intestinal permeation. In *Pharmacology of intestinal permeation* (ed. TZ Csaky), pp. 165–269. New York, NY: Springer.
10. Debnam ES, Levin RJ. 1975 Effects of fasting and semi-starvation on the kinetics of active and passive sugar absorption across the small intestine *in vivo*. *J. Physiol.* **252**, 681–700.
11. Winne D. 1978 Dependence of intestinal absorption *in vivo* on the unstirred layer. *Naunyn. Schmiedebergs Arch. Pharmacol.* **304**, 175–181. (doi:10.1007/BF00495554)
12. Winne D, Kopf S, Ulmer ML. 1979 Role of unstirred layer in intestinal absorption of phenylalanine *in vivo*. *Biochim. Biophys. Acta* **550**, 120–130. (doi:10.1016/0005-2736(79)90120-2)
13. Fagerholm U, Lennernäs H. 1995 Experimental estimation of the effective unstirred water layer thickness in the human jejunum, and its importance in oral drug absorption. *Eur. J. Pharm. Sci.* **3**, 247–253. (doi:10.1016/0928-0987(95)00027-B)
14. Pohl P, Saparov SM, Antonenko YN. 1998 The size of the unstirred layer as a function of the solute diffusion coefficient. *Biophys. J.* **75**, 1403–1409. (doi:10.1016/S0006-3495(98)74058-5)
15. Sellers LA, Allen A, Morris ER, Ross-Murphy SB. 1991 The rheology of pig small intestinal and colonic mucus: weakening of gel structure by non-mucin components. *Biochim. Biophys. Acta* **1115**, 174–179. (doi:10.1016/0304-4165(91)90027-E)
16. Smithson KW, Millar DB, Jacobs LR, Gray GM. 1981 Intestinal diffusion barrier: unstirred water layer or membrane surface mucous coat? *Science* **214**, 1241–1244. (doi:10.1126/science.7302593)
17. Szentkuti L, Lorenz K. 1995 The thickness of the mucus layer in different segments of the rat intestine. *Histochem. J.* **27**, 466–472.
18. Atuma C, Strugala V, Allen A, Holm L. 2001 The adherent gastrointestinal mucus gel layer: thickness and physical state *in vivo*. *Am. J. Physiol.* **280**, G922–G929.
19. Sugano K. 2009 Estimation of effective intestinal membrane permeability considering bile micelle solubilisation. *Int. J. Pharm.* **368**, 116–122. (doi:10.1016/j.ijpharm.2008.10.001)
20. Suh J, Dawson M, Hanes J. 2005 Real-time multiple-particle tracking: applications to drug and gene delivery. *Adv. Drug Deliv. Rev.* **57**, 63–78. (doi:10.1016/j.addr.2004.06.001)
21. Swidsinski A, Loening-Baucke V, Theissig F, Engelhardt H, Bengmark S, Koch S, Lochs H, Doerffel Y. 2007 Comparative study of the intestinal mucus barrier in normal and inflamed colon. *Gut* **56**, 343–350. (doi:10.1136/gut.2006.098160)
22. Danielsen EM, Sjöström H, Norén O, Bro B, Dabelsteen E. 1982 Biosynthesis of intestinal microvillar proteins. Characterization of intestinal explants in organ culture and evidence for the existence of pro-forms of the microvillar enzymes. *Biochem. J.* **202**, 647–654.
23. Ham AW. 1974 *Histology*, 7th edn. Philadelphia: Lippincott.
24. Weinstein LD, Shoemaker CP, Hersh T, Wright HK. 1969 Enhanced intestinal absorption after small bowel resection in man. *Arch. Surg.* **99**, 560–562. (doi:10.1001/archsurg.1969.01340170012003)

25. Lentle RG, Hemar Y, Hall CE, Stafford KJ. 2005 Periodic fluid extrusion and models of digesta mixing in the intestine of a herbivore, the common brushtail possum (*Trichosurus vulpecula*). *J. Comp. Physiol.* **B175**, 337–347.
26. MacKintosh FC, Schmidt CF. 1999 Microrheology. *Curr. Opin. Colloid. Interface Sci.* **4**, 300–307. (doi:10.1016/S1359-0294(99)90010-9)
27. Macierzanka A, Rigby NM, Corfield AP, Wellner N, Böttger F, Mills ENC, Mackie AR. 2011 Adsorption of bile salts to particles allows penetration of intestinal mucus. *Soft Matter* **7**, 8077–8084. (doi:10.1039/c1sm05888f)
28. Dawson M, Wirtz D, Hanes J. 2003 Enhanced viscoelasticity of human cystic fibrotic sputum correlates with increasing microheterogeneity in particle transport. *J. Biol. Chem.* **278**, 50 393–50 401. (doi:10.1074/jbc.M309026200)
29. Crater JS, Carrier RL. 2010 Barrier properties of gastrointestinal mucus to nanoparticle transport. *Macromol. Biosci.* **10**, 1473–1483. (doi:10.1002/mabi.201000137)
30. Rogers SS, Waigh TA, Zhao X, Lu JR. 2007 Precise particle tracking against a complicated background: polynomial fitting with Gaussian weight. *Phys. Biol.* **4**, 220–227. (doi:10.1088/1478-3975/4/3/008)
31. Gardel ML, Valentine MT, Weitz DA. 2005 Microrheology. In *Microscale diagnostic techniques* (ed. KS Breuer), pp. 1–50. Berlin, Germany: Springer.
32. Waigh TA. 2005 Microrheology of complex fluids. *Rep. Prog. Phys.* **68**, 685–742. (doi:10.1088/0034-4885/68/3/R04)
33. Mason TG. 2000 Estimating the viscoelastic moduli of complex fluids using the generalized Stokes–Einstein equation. *Rheol. Acta* **39**, 371–378. (doi:10.1007/s003970000094)
34. Lentle RG, Janssen PWM. 2011 Flow, mixing and absorption at the mucosa. In *Physical processes of digestion* (eds RG Lentle, PWM Janssen), pp. 234–294. New York, NY: Springer.
35. Taylor C, Allen A, Dettmar PW, Pearson JP. 2003 The gel matrix of gastric mucus is maintained by a complex interplay of transient and nontransient associations. *Biomacromolecules* **4**, 922–927. (doi:10.1021/bm025767t)
36. Valentine MT, Kaplan PD, Thota D, Crocker JC, Gisler T, Prud'homme RK, Beck M, Weitz DA. 2001 Investigating the microenvironments of inhomogeneous soft materials with multiple particle tracking. *Phys. Rev. E* **64**, 1–9.
37. Lai SK, O'Hanlon DE, Harrold S, Man ST, Wang YY, Cone R, Hanes J. 2007 Rapid transport of large polymeric nanoparticles in fresh undiluted human mucus. *Proc. Natl Acad. Sci. USA* **104**, 1482–1487. (doi:10.1073/pnas.0608611104)
38. Olmsted SS, Padgett JL, Yudin AI, Whaley KJ, Moench TR, Cone RA. 2001 Diffusion of macromolecules and virus-like particles in human cervical mucus. *Biophys. J.* **81**, 1930–1937. (doi:10.1016/S0006-3495(01)75844-4)
39. Williams MAK, Vincent RR, Pinder DN, Hemar Y. 2008 Microrheological studies offer insights into polysaccharide gels. *J. Non-Newtonian Fluid Mech.* **149**, 63–70. (doi:10.1016/j.jnnfm.2007.05.006)
40. de Gennes PG. 1971 Reptation of a polymer chain in the presence of fixed obstacles. *J. Chem. Phys.* **55**, 572–579. (doi:10.1063/1.1675789)
41. Cone RA. 2009 Barrier properties of mucus. *Adv. Drug Deliv. Rev.* **61**, 75–85. (doi:10.1016/j.addr.2008.09.008)
42. Sawaguchi A, Ishihara K, Kawano J, Oinuma T, Hotta K, Suganuma T. 2002 Fluid dynamics of the excretory flow of zymogenic and mucin contents in rat gastric gland processed by high-pressure freezing/freeze substitution. *J. Histochem. Cytochem.* **50**, 223–234. (doi:10.1177/002215540205000210)
43. Matsuo K, Ota H, Akamatsu T, Sugiyama A, Katsuyama T. 1997 Histochemistry of the surface mucous gel layer of the human colon. *Gut* **40**, 782–789. (doi:10.1136/gut.40.6.782)
44. Swidsinski A, Sydora BC, Doerffel Y, Loening-Baucke V, Vaneechoutte M, Lupicki M, Scholze J, Lochs H, Dieleman LA. 2007 Viscosity gradient within the mucus layer determines the mucosal barrier function and the spatial organization of the intestinal microbiota. *Inflamm. Bowel Dis.* **13**, 963–970. (doi:10.1002/ibd.20163)
45. Verdugo P. 1990 Goblet cells secretion and mucogenesis. *Annu. Rev. Physiol.* **52**, 157–176. (doi:10.1146/annurev.ph.52.030190.001105)
46. Whitaker M, Zimmerberg J. 1987 Inhibition of secretory granule discharge during exocytosis in sea urchin eggs by polymer solutions. *J. Physiol.* **389**, 527–539.
47. Chandler DE, Whitaker M, Zimmerberg J. 1989 High molecular weight polymers block cortical granule exocytosis in sea urchin eggs at the level of granule matrix disassembly. *J. Cell Biol.* **109**, 1269–1278. (doi:10.1083/jcb.109.3.1269)
48. Verdugo P. 1993 Polymer gel phase transition in condensation–decondensation of secretory products. *Adv. Polym. Sci.* **110**, 145–156. (doi:10.1007/BFb0021131)
49. Jeffery PK, Li D. 1997 Airway mucosa: secretory cells, mucus and mucin genes. *Eur. Respir. J.* **10**, 1655–1662. (doi:10.1183/09031936.97.10071655)
50. Davis CW, Dowell ML, Lethem M, Van Scott M. 1992 Goblet cell degranulation in isolated canine tracheal epithelium: response to exogenous ATP, ADP, and adenosine. *Am. J. Physiol.* **262**, C1313–C1323.
51. Lethem M, Dowell M, Van Scott M, Yankaskas J, Egan T, Boucher R, Davis C. 1993 Nucleotide regulation of goblet cells in human airway epithelial explants: normal exocytosis in cystic fibrosis. *Am. J. Respir. Cell Mol. Biol.* **9**, 315.
52. McConnell RE, Higginbotham JN, Shifrin Jr DA, Tabb DL, Coffey RJ, Tyska MJ. 2009 The enterocyte microvillus is a vesicle-generating organelle. *J. Cell Biol.* **185**, 1285–1298. (doi:10.1083/jcb.200902147)
53. Dawson M, Krauland E, Wirtz D, Hanes J. 2004 Transport of polymeric nanoparticle gene carriers in gastric mucus. *Biotechnol. Prog.* **20**, 851–857. (doi:10.1021/bp0342553)
54. Lentle RG, De Loubens C, Hulls C, Janssen PWM, Golding MD, Chambers JD. 2012 Organization of longitudinal and circular contractions during pendular and segmental activity; a comparison of duodenal contractile activity in the rat and guinea pig. *Neurogastroenterol. Mot.* **24**, 686–695, e298. (doi:10.1111/j.1365-2982.2012.01923.x)
55. Grivel ML, Ruckebusch Y. 1972 The propagation of segmental contractions along the small intestine. *J. Physiol.* **227**, 611–625.
56. Robbe C, Capon C, Maes E, Rousset M, Zweibaum A, Zanetta JP, Michalski JC. 2003 Evidence of regio-specific glycosylation in human intestinal mucins. *J. Biol. Chem.* **278**, 46 337–46 348. (doi:10.1074/jbc.M302529200)
57. Kararli TT. 1995 Comparison of the gastrointestinal anatomy, physiology, and biochemistry of humans and commonly used laboratory animals. *Biopharm. Drug Dispos.* **16**, 351–380. (doi:10.1002/bdd.2510160502)
58. Boshi Y *et al*. 1996 Developmental changes in distribution of the mucous gel layer and intestinal permeability in rat small intestine. *J. Parenter. Enteral Nutr.* **20**, 406–411. (doi:10.1177/0148607196020006406)